Science Translational Medicine
AAAS

www.sciencetranslationalmedicine.org/cgi/content/full/8/361/361ra139/DC1

Supplementary Materials for

NAD$^+$ repletion improves muscle function in muscular dystrophy and counters global PARylation

Dongryeol Ryu, Hongbo Zhang, Eduardo R. Ropelle, Vincenzo Sorrentino, Davi A. G. Mázala, Laurent Mouchiroud, Philip L. Marshall, Matthew D. Campbell, Amir Safi Ali, Gary M. Knowels, Stéphanie Bellemin, Shama R. Iyer, Xu Wang, Karim Gariani, Anthony A. Sauve, Carles Cantó, Kevin E. Conley, Ludivine Walter, Richard M. Lovering, Eva R. Chin, Bernard J. Jasmin, David J. Marcinek, Keir J. Menzies,* Johan Auwerx*

*Corresponding author. Email: admin.auwerx@epfl.ch (J.A.); kmenzies@uottawa.ca (K.J.M.)

Published 19 October 2016, *Sci. Transl. Med.* **8**, 361ra139 (2016)
DOI: 10.1126/scitranslmed.aaf5504

This PDF file includes:

Detailed conditions and analysis of MRS data:

Peak simulations: Solutions emulating in vivo conditions were prepared with NAD^+ and $NADP^+$ using binding constants taken from the USA National Institute of Standards and Technology (NIST) Critically Selected Stability Constants of Metal Complexes Database (see (*56*)). All solutions contained (in mmol/L): EGTA 15, MOPS 80, free Mg^{2+} 1, Na^+ 83 and K^+ 52. The following were varied in individual solutions: ATP, ADP, P_i, Creatine Phosphate (PCr), ADP, NAD^+, NADH, $NADP^+$, or UDP-Glucose. The ionic strength was maintained at 0.175M, pH = 7.0 (36°C) in all solutions. High-resolution MR spectra of solutions in an NMR tube were taken at 4.7T (sweep width=10,000 Hz, 16K complex points, 128 FIDs, 5 sec delay between pulses). The Spin Simulation feature of the Mnova software provided the NAD^+ (-10.74 ppm and J coupling, 20.03 Hz) and $NADP^+$(-10.83 ppm and J coupling, 18.03 Hz) resonances at each field based on the spin parameters and chemical shifts at 4.7T as described (*57*).
Metabolite Concentrations: Mice were euthanized within 20 minutes of the end of the MRS experiment. Gastrocnemius muscles were removed and frozen from anesthetized mice within 20 minutes of the end of the MRS experiments. Concentration of ATP was measured in the gastrocnemius muscle by HPLC (Waters, Milford, MA) using a protocol described in detail elsewhere (*58*).

Analyses of in vivo *ATP Fluxes:* ^{31}P MR spectra were exponentially multiplied (40 Hz at 14T), fourier transformed, and manually phase corrected using Bruker TopSpin (14T) software. Fully relaxed and dynamic phase spectra were then analyzed with custom written MATLAB software (Mathworks, Natick, MA).
The method used for analyzing MR spectra is described in detail elsewhere (*51*). Peak areas relative to gamma a-ATP peak area from fully relaxed spectra were used to calculate the resting inorganic phosphate P_i/ATP and PCr/ATP ratios. Three consecutive dynamic spectra were summed to improve signal-to-noise ratio before using the Fit-to-Standard algorithm (*59*) to determine PCr and P_i peak magnitudes throughout dynamic acquisition, relative to rest. Absolute PCr and P_i concentrations were calculated using the ATP concentration measured by HPLC. The chemical shift between the P_i and PCr peaks was used to calculate the cellular pH during the dynamic phase (*60*). Experiments where end of ischemia pH fell below 6.8 were excluded from analyses of ATPmax.

NAD^+ in vivo*:* The NAD(P) region (-10.4 to -11.3 ppm) was extracted from the fully relaxed spectra by fitting a Lorenztian line shape to the a-ATP peak. The NAD^+ and $NADP^+$ peaks were estimated by a least squares fit of the simulated peaks to the -10.4 to -11.0 ppm portion of the extracted region.

Supplementary Figures

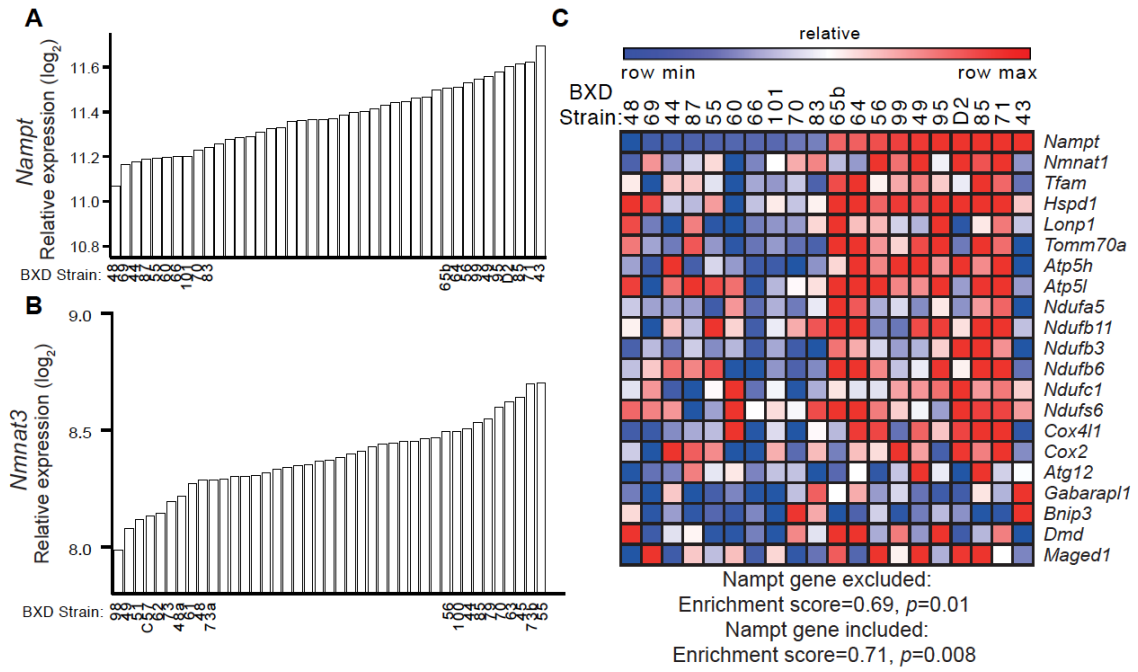

Fig. S1. Enrichment of mitochondrial-related transcripts with *Nampt* expression in genetically diverse BXD mice. Expression of (**A**) *Nampt* and (**B**) *Nmnat3* in the quadriceps of 42 strains of the BXD mouse genetic reference population. Each bar represents mRNA from a pool of 5 animals per strain. Extreme strains are labeled. Custom gene set analysis showing enrichment of mitochondrial-related transcripts with (**C**) *Nampt* in data from strains with the 10 highest and 10 lowest transcript levels from 42 strains of the BXDs (*20*). Using gene set enrichment analysis we found a positive correlation to *Nampt* transcript expression with an enrichment score=0.69 and *P*=0.01, with the *Nampt* gene excluded from the analysis.

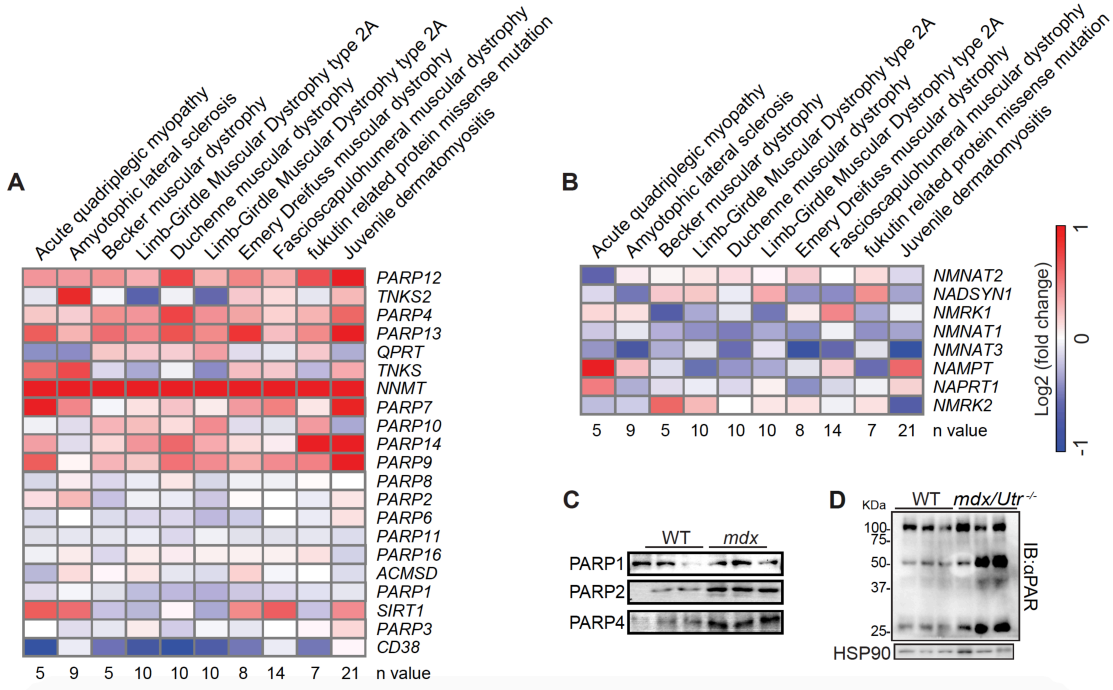

Fig. S2. **Expression of NAD$^+$-related transcripts in human muscle and PARP protein expression and PARylation in mouse models of muscular dystrophy.** The expression of transcripts related to NAD$^+$ (**A**) consumption or (**B**) biosynthesis exhibit an enrichment signature of *PARP* genes and the *NNMT* gene that is consistent across skeletal muscle datasets (*24, 25*) from a variety of muscular dystrophies and in patients with (neuro)-muscular diseases. All results for a given condition are averaged from a group of datasets and expressed in relationship to the average of the control patient values (n value for each disease is indicated at the bottom of the heatmap; n=18 for the control group). (**C**) PARP1 (WT=1.00±0.42, *mdx*=1.41±0.36), PARP2 (WT=1.00±0.56, *mdx*=3.54±0.24, *P*=0.014) and PARP4 (WT=1.00±0.28, *mdx*=2.29±0.02, *P*=0.036) proteins were induced in *mdx* mice. HSP90 (Fig. 4D) was used as loading control. (**D**) Total PARylation content (WT=1.00±0.41, *mdx*/*Utr*$^{-/-}$ = 2.09±0.71) was increased in *mdx*/*Utr*$^{-/-}$ gastrocnemius muscle.

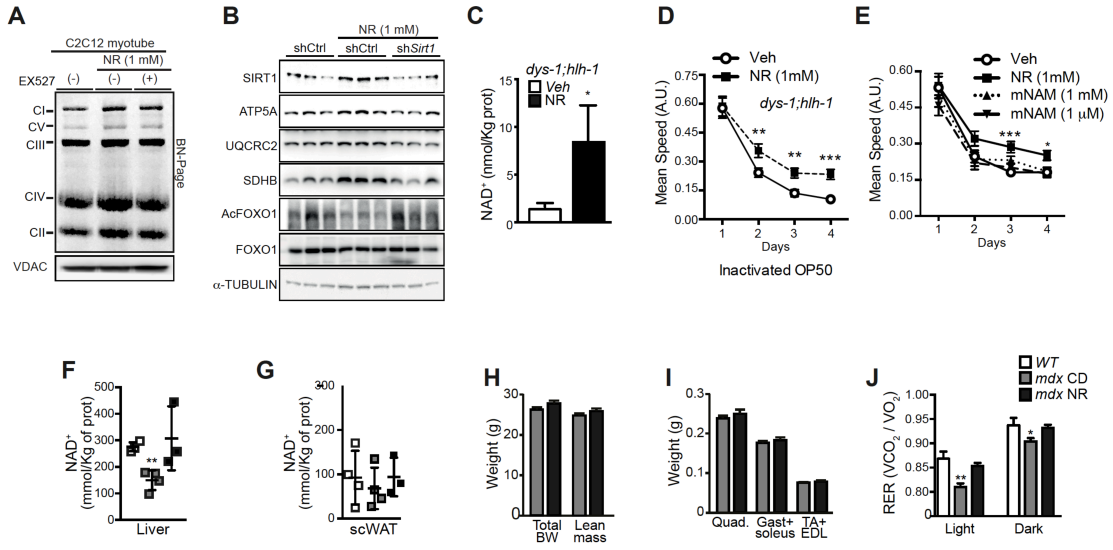

Fig. S3. **NR enhances mitochondrial content in C2C12 myotubes and improves function in *dys-1;hlh-1* double mutant *C. elegans*.** C2C12 myotubes were treated with 0.5 to 1 mM NR. 12 hrs of NR induces (**A**) mitochondrial biogenesis in the presence or absence of EX527, as demonstrated by Blue-native PAGE of mitochondrial complexes from isolated mitochondria. (**B**) sh*Sirt1* adenovirus infection of myotubes attenuated increases in mitochondrial proteins (ATP5A (shCtrl=1.00±0.17, shCtrl+NR=1.41±0.16, sh*Sirt1*+NR=1.17±0.42), UQCRC2 (shCtrl=1.00±0.06, shCtrl+NR=1.13±0.02, sh*Sirt1*+NR=0.45±0.10, shCtrl+NR vs. sh*Sirt1*+NR P=0.002), SDHB (shCtrl=1.00±0.34, shCtrl+NR=2.16±0.02, sh*Sirt1*+NR=1.42±0.72, shCtr vs. shCtrl+NR P=0.028)) and reductions in FOXO1 acetylation (shCtrl=1.00±0.21, shCtrl+NR=0.22±0.07, sh*Sirt1*+NR=1.36±0.23, shCtr vs. shCtrl+NR P=0.023, shCtrl+NR vs. sh*Sirt1*+NR P=0.009) following NR treatment. (**C**) NAD^+ levels are significantly elevated by 2 days of NR treatment in *dys-1;hlh-1* mutant worms (n=4, 1000 worms per experiment). Improvements in *dys-1;hlh-1* mutant worm fitness on days 1-4 of adulthood in worms fed (**D**) a diet of heat inactivated OP50 with NR (1mM), or (**E**) a live OP50 diet with NR (1mM) or mNAM (1mM or 1μM), as measured by examining worm motility using the worm tracker (n=3, 60 worms per experiment). *mdx* mice treated for 12 weeks with NR demonstrated (**F**) restored NAD^+ levels in liver (n=4 for WT and *mdx* CD, n=3 for *mdx* NR) yet (**G**) no changes in NAD^+ in subcutaneous WAT (n=4 for WT and *mdx* CD, n=3 for *mdx* NR). NR treated *mdx* mice also showed no significant changes in (**H**) total body weight, lean mass (n=6) or (**I**) wet weights of quadriceps, gastrocnemius and soleus or tibialis anterior and extensor digitorum longus muscles (n=5). (**J**) Energy expenditure was evaluated through calculation of the respiratory exchange ratio (RER) over a 24 hr period for *mdx* mice with or without NR treatment compared to WT mice (n=6).

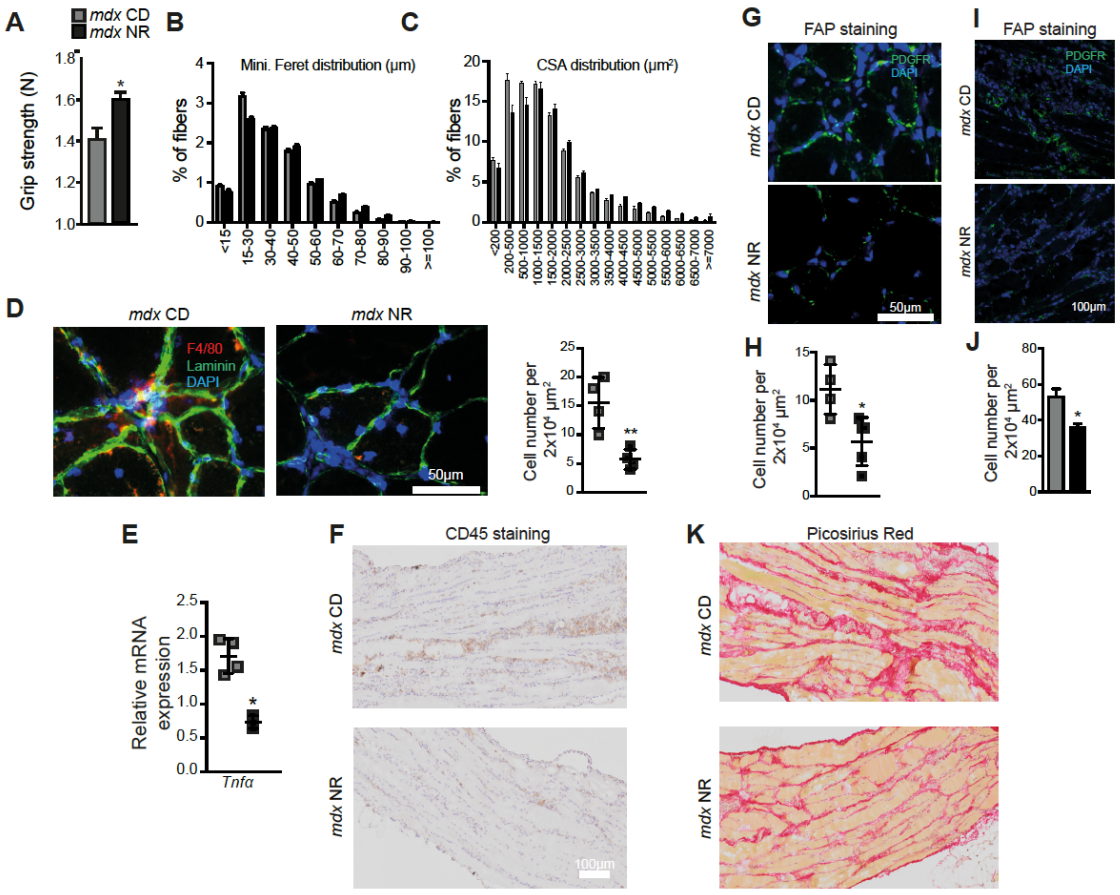

Fig. S4. Improvements in the phenotype of NR-treated *mdx* mice. *mdx* mice treated for 12 weeks with NR exhibited (**A**) increased limb grip strength (Newtons of force, n=6). Analysis of the (**B**) minimal Feret's diameter (in µm) and the (**C**) cross-sectional area (in μm^2) of *mdx* tibialis anterior muscle fibers show an increase in fiber size with NR treatment (8 weeks of NR treatment, n=5). Quantification of images was performed with ImageJ software. NR-treated *mdx* mice also demonstrated (**D**) reduced macrophage content, quantified by counting F40/80-positive stained cells in *mdx* tibialis anterior muscles (n=4). Quantification of images was performed with ImageJ software. (**E**) mRNA levels of *tnfα,* a mediator of inflammation in *mdx* mice, was attenuated with NR treatment in gastrocnemius muscle (n=3). (**F**) CD45 positive cells were reduced in the longitudinal-sections of NR-treated *mdx* mouse diaphragms. PDGFR positive cells were reduced following NR in both (**G**) transverse-sections of TA muscle and (**H**) quantified transverse-sections of diaphragms in *mdx* mice. Quantification of images was performed with ImageJ software (n=4, *mdx*; n=5, *mdx* NR). (**I**) Reduced PGDFR staining of longitudinal-sections of the diaphragm (**J**) quantified using ImageJ software (n=6, *mdx*; n=5, *mdx* NR). (**K**) Fibrosis was reduced in longitudinal sections of the diaphragm in *mdx* mice given an NR supplemented diet, as seen with less picosirius red staining.

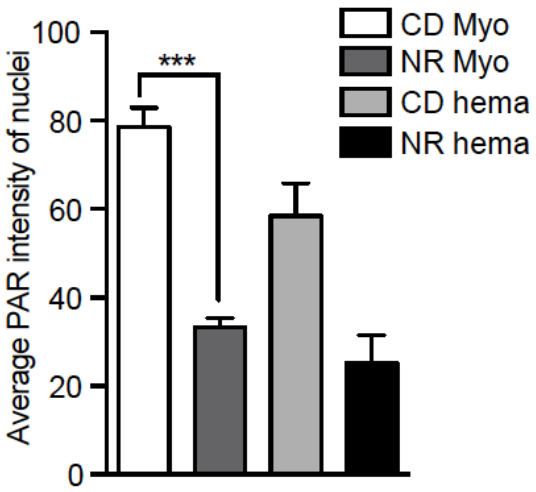

Fig. S5. Average intensity of nuclei immunohistochemically stained with anti-PAR antibody. Skeletal muscle nuclei stained from *mdx* mice with anti-PAR are differentiated from the inflammatory cell fraction using an anti-CD45 counterstain (n=3, *CD*; n=3, NR). Quantification of images was performed with ImageJ software.

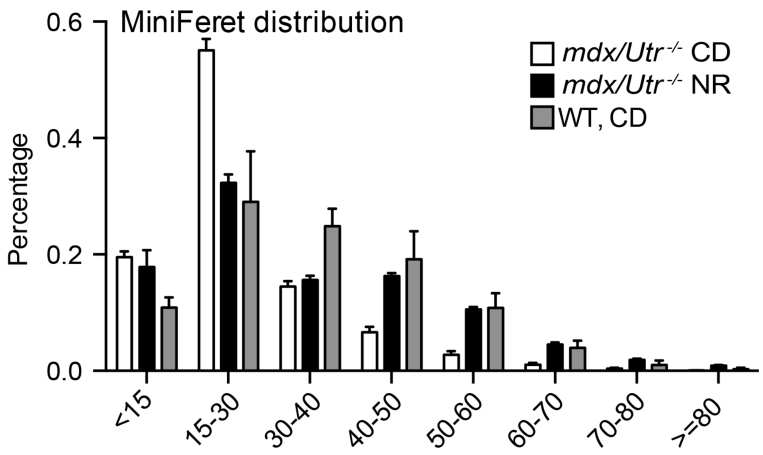

Fig. S6. **Increases in the minimal Feret's diameter of *mdx/Utr*$^{-/-}$ mouse muscle fibers treated with NR.** 10-week-old *mdx/Utr*$^{-/-}$ mice received a dietary supplement with NR (400 mg/kg/day) for 8 weeks. Images stained with Dapi and laminin were used to quantify increases in the distribution of minimal Feret's diameter (in µm) of fibers in tibialis anterior muscles of NR treated *mdx*/*Utr*$^{-/-}$ mice (n=3, *mdx*/*Utr*$^{-/-}$; n=3, *mdx*/*Utr*$^{-/-}$ NR; n=3, WT, CD). Quantification of images was performed with ImageJ software.

Table S1: Primer sets for qRT-PCR analyses

Gene	Description	Forward Primer	Reverse Primer
36b4	Ribosomal protein, large, P0	AGATTCGGGATATGCTGTTGG	AAAGCCTGGAAGAAGGAGGTC
B2m	Beta-2 microglobulin	TTCTGGTGCTTGTCTCACTG	TATGTTCGGCTTCCCATTCT
Gapdh	Glyceraldehyde-3-phosphate dehydrogenase	TGTGTCCGTCGTGGATCTGA	CCTGCTTCACCACCTTCTTGAT
Tnfα	Tumor necrosis factor	GTAGCCCACGTCGTAGCAAAC	GCAGACTTACTGACCAGCTCAGA
Il13	Interleukin 13	CACACTCCATACCATGCTGC	TGTGTCTCTCCCTCTGACCC
Il4	Interleukin 4	ACAGGAGAAGGGACGCCAT	GAAGCCCTACAGACGAGCTCA
Ndufa2	NADH dehydrogenase (ubiquinone) 1 alpha subcomplex, 2	GCACACATTTCCCCACACTG	CCAACCTGCCCATTCTGAT
Sdhb	Succinate dehydrogenase complex, subunit B	GGACCTATGGTGTTGGATGC	GTGTGCACGCCAGAGTATTG
ATP5g1	ATP synthase, H+ transporting, mitochondrial F0 complex, subunit C1 (subunit 9)	GCTGCTTGAGAGATGGTTC	AGTTGGTGTGGCTGGATCA
Nmnat1	Nicotinamide nucleotide adenylyltransferase 1	TGTGCCCAAGGTGAAATTGCT	CCACGATTTGCGTGATGTCC
Uqcrc1	Ubiquinol-cytochrome c reductase core protein 1	AGACCCAGGTCAGCATCTTG	GCCGATTCTTTGTTCCCTTGA
Sirt1	Sirtuin 1	GCTGACGACTTCGACGACG	TCGGTCAACAGGAGGTTGTCT